Ion mobility-mass spectrometry and collision induced unfolding of designed bispecific antibody therapeutics

Rosendo C. Villafuerte-Vega,† Henry W. Li†, Thomas R. Slaney,‡ Naresh Chennamsetty,‡ Guodong Chen,‡ Li Tao,‡ and Brandon T. Ruotolo*†

† Department of Chemistry, University of Michigan, Ann Arbor, Michigan 48109, United States

‡ Analytical Development and Attribute Sciences, Biologics Development, Global Product Development and Supply, Bristol Myers Squibb, New Brunswick, New Jersey 08903, United States

ABSTRACT: Bispecific antibodies (bsAbs) represent a critically important class of emerging therapeutics capable of targeting two different antigens simultaneously. As such, bsAbs have been developed as effective treatment agents for diseases that remain challenging for conventional monoclonal antibody (mAb) therapeutics to access. Despite these advantages, bsAbs are intricate molecules, requiring both the appropriate engineering and pairing of heavy and light chains derived from separate parent mAbs. Current analytical tools for tracking the bsAb construction process have demonstrated a limited ability to robustly probe the higher order structure (HOS) of bsAbs. Native ion mobility-mass spectrometry (IM-MS) and collision induced unfolding (CIU) have proven to be useful tools in probing the HOS of mAb therapeutics. In this report, we describe a series of detailed and quantitative IM-MS and CIU datasets that reveal HOS details associated with a knob-into-hole (KiH) bsAb model system and its corresponding parent mAbs. We find that quantitative analysis of CIU data indicates that global KiH bsAb stability occupies an intermediate space between the stabilities recorded for its parent mAbs. Furthermore, our CIU data identifies the hole-containing half of the KiH bsAb construct to be least stable, thus driving much of the overall stability of the KiH bsAb. An analysis of both intact bsAb and enzymatic fragments allows us to associate the first and second CIU transitions observed for the intact KiH bsAb to the unfolding Fab and Fc domains, respectively. This result is likely general for CIU data collected for low charge state mAb ions and is supported by data acquired for deglycosylated KiH bsAb and mAb constructs, each of which indicate greater destabilization of the second CIU transition observed in our data. When integrated, our CIU analysis allows us to link changes in the first CIU transition primarily to the Fab region of the hole-containing halfmer, while the second CIU transition is likely strongly connected to the Fc region of the knob-containing halfmer. Taken together, our results provide an unprecedented roadmap for evaluating the domain-level stabilities and HOS of both KiH bsAb and mAb constructs using CIU.

Introduction

Bispecific antibodies (bsAbs) have become promising therapeutic modalities since they merge the specificities of two different monoclonal antibodies (mAbs). This unique quality of bsAbs not only permits the targeting of two distinct epitopes or antigens simultaneously, but it also paves the way for innovative functionalities that are unattainable with conventional mAb-based therapeutics. Examples of such treatment strategies include the redirection and activation of immune effector cell cytotoxic activity to specifically eradicate tumor cells,[1–3] the selective inhibition of enzymes across the blood brain barrier responsible for amyloid-β (Aβ) peptide production,[4,5] and the dual targeting and neutralization of two independent growth factors associated with neovascular eye diseases.[6,7] These therapeutic capabilities have led to the market approval of two bsAbs by the US Food and Drug Administration, while well over 100 bsAbs are currently in clinical development.[8]

Advancements in antibody engineering and development have cultivated many different commercialized technology platforms within pharmaceutical and biotechnology companies for novel bsAb construction.[9] These technologies have led to the generation of primarily two different architectural classes of bsAbs: 1) fragment-based formats that join various antigen-binding moieties into one entity without a fragment crystallizable (Fc) region and 2) immunoglobulin G (IgG)-like molecules containing two different fragment antigen-binding (Fab) regions connected by an Fc domain. In most cases, the latter 'IgG format' for bsAbs exhibits greater solubility, stability, and plasma half-life when compared to other constructs due to its large size and resistance to catabolism by the neonatal Fc receptor, FcRn.[10] However, the production of bsAbs using this format is challenging since dual specificity is dependent on the co-expression of variable domains from two separate light chains and two separate heavy chains. Therefore, one of the major challenges is the chain association issue, where different chain combinations can theoretically result in 10 different antibodies of which only one matches the target functional bsAb.[9,11]

Protein engineering approaches, such as the "knobs-into-holes" (KiH) concept, have been developed to address

the bsAb chain association problem and enforce the proper heterodimerization of engineered heavy chains. This design strategy involves the mutation of amino acid residues at the interface between C_H3 domains of each heavy chain, where targeted residues are replaced with bulkier amino acids in the "knob" variant and smaller amino acids in the "hole" variant.[12] However, the characterization of bsAb therapeutics extends beyond their proper assembly. Antibody therapeutics are large (~150 kDa), exhibiting significantly more structural complexity and heterogeneity than conventional small molecule drugs. Additionally, changes in higher order structure (HOS) caused by KiH engineering, post-translational modifications, or degradation can result in the inhibition of molecular binding, an increased potential for immunogenicity, and a higher rate of aggregation.[13–16] Therefore, a thorough characterization of KiH bsAb HOS is crucial not only to define bsAb structure-function relationships but also to ensure stability, efficacy, and safety of the final therapeutic.[17,18]

A comprehensive range of biophysical techniques have been well-established for the characterization of mAb therapeutic HOS and stability. Tools such as circular dichroism (CD),[19] differential scanning calorimetry (DSC),[20] and size exclusion chromatography (SEC)[21] offer a global perspective on mAb stability and conformation, but they lack the resolution needed to distinguish subtle conformational changes. By contrast, techniques such as nuclear magnetic resonance (NMR) spectroscopy,[22] X-ray crystallography,[23] and cryogenic electron microscopy (cryo-EM)[24] provide atomically resolved structural information, but they typically require extensive sample preparation, large quantities of homogenous sample, lengthy data acquisition times, and complex data interpretation.[25] Currently, no full-length IgG-like bsAb crystal structures are publicly available, and only bsAb fragment structures have been reported.[26,27]

Recently, native ion mobility-mass spectrometry (IM-MS) has emerged as a useful structural biology tool capable of probing the HOS of mAb therapeutics from a few micrograms of sample in the presence of structural heterogeneity and impurities. IM separates gas-phase protein ions based on their charge and rotationally averaged collision cross sections (CCSs) on the millisecond timescale.[28] When coupled with MS, two ions of the same mass-to-charge ratio but different CCSs can be readily distinguished. IM-MS measurements have been shown to monitor the dynamics of bsAb formation resulting from Fab-arm exchange (FAE),[29] resolve disulfide structural isoforms of IgG2 mAbs,[30] and assess antibody-drug conjugate (ADC) structural heterogeneity.[31] Moreover, collision induced unfolding (CIU) has enabled IM-MS to synchronously provide both protein structure and conformational stability information.[32] In CIU experiments, protein ions are collisionally-heated prior to IM separation to elicit protein unfolding in the gas-phase. CIU has discriminated differences based on disulfide patterns,[33] glycosylation levels,[34,35] domain exchanging properties,[36] and drug conjugation.[37,38] CIU has also probed a bsAb formed via FAE of wt-IgG4s, highlighting that such bsAb can retain structural information from both its parent mAbs.[39] Despite past progress, quantitative CIU has yet to be deployed in the HOS evaluation of engineered KiH bsAb modalities, and the individual contributions of parent mAbs to bsAb HOS remain unclear.

In this report, we describe the first application of quantitative CIU to real-world, engineered bsAbs. Specifically, we extend the capabilities of native IM-MS and CIU to robustly characterize the HOS of a model KiH bsAb and its parent 'knob' and 'hole' homodimer mAbs. We define biophysical connections between these constructs by quantifying the global differences observed between CIU fingerprints and comparing their stabilities. We further convert the bsAb and its parent mAbs into fragments of various types to evaluate their domain-level stabilities. By comparing the stabilities of isolated domains, we can localize contributions from each parent mAb in our KiH bsAb CIU transitions, where we discover evidence of Fab domains unfolding in lower-energy CIU transitions. After enzymatically removing *N*-linked glycans from the Fc regions of our constructs, we find evidence of destabilization occurring primarily in higher-energy CIU transitions, permitting us to pinpoint the unfolding of the Fc region in our CIU fingerprints. We conclude by discussing the potential impact of native IM-MS and CIU workflows on the HOS characterization of KiH bsAbs.

Experimental Section

Sample Preparation. KiH bsAb heterodimer (10 mg/mL) and 'knob' and 'hole' homodimer mAbs (2 mg/mL) were produced, purified, and formulated in their respective formulation buffer at Bristol Myers Squibb (New Brunswick, NJ). Here, we define 'homodimer' as intact mAb containing either 'knob' or 'hole' mutations, 'halfmer' as the half-molecule of 'knob' and 'hole' homodimer mAbs, and 'heterodimer' as intact KiH bsAb formed from the dimerization of 'knob' and 'hole' halfmers. All antibodies studied here were of the IgG isotype and IgG2 subclass, where one disulfide bond in the hinge region was mutated out. Glycerol-free PNGase F (500,000 units/mL) was purchased from New England Biolabs (Ipswich, MA). Papain from papaya latex was supplied as a buffered aqueous suspension and acquired from Sigma Aldrich (St. Louis, MO).

All native, unmodified samples were buffer exchanged into 200 mM ammonium acetate (pH 6.8 – 7.0) using Micro Bio-Spin P-6 columns (Bio-Rad, Hercules, CA) and diluted to working concentrations of 1 mg/mL (~6.7 μM) of intact homodimer or heterodimer. Removal of *N*-glycans from antibody constructs was achieved using PNGase F under non-denaturing conditions overnight per the vendor's recommended protocol. A control without PNGase F was incubated concurrently. For the papain digestion of the KiH bsAb, papain was first activated with 5 mM cysteine for 30 min at 37°C. Excess cysteine was then removed by buffer exchanging the activated papain into digestion buffer (200 mM ammonium acetate, 5 mM EDTA, pH 6.8 – 7.0) using Micro Bio-Spin P-6 columns. KiH bsAb (1 mg/mL) sample was buffer exchanged into digestion buffer followed by the addition of activated papain to achieve a 1:100 (papain:bsAb) ratio. The digest was then incubated for 2 hr at 37°C to cleave the KiH bsAb above the hinge region and generate intact Fab and Fc fragments. A control without papain was also incubated to track potential disulfide bond reduction caused by any residual cysteine in the digestion buffer. Little to no disulfide bond reduction was observed. All deglycosylated and papain-digested samples were quenched on ice and immediately buffer exchanged into 200 mM ammonium acetate (pH 6.8 – 7.0) using Bio-Spin P-6 columns.

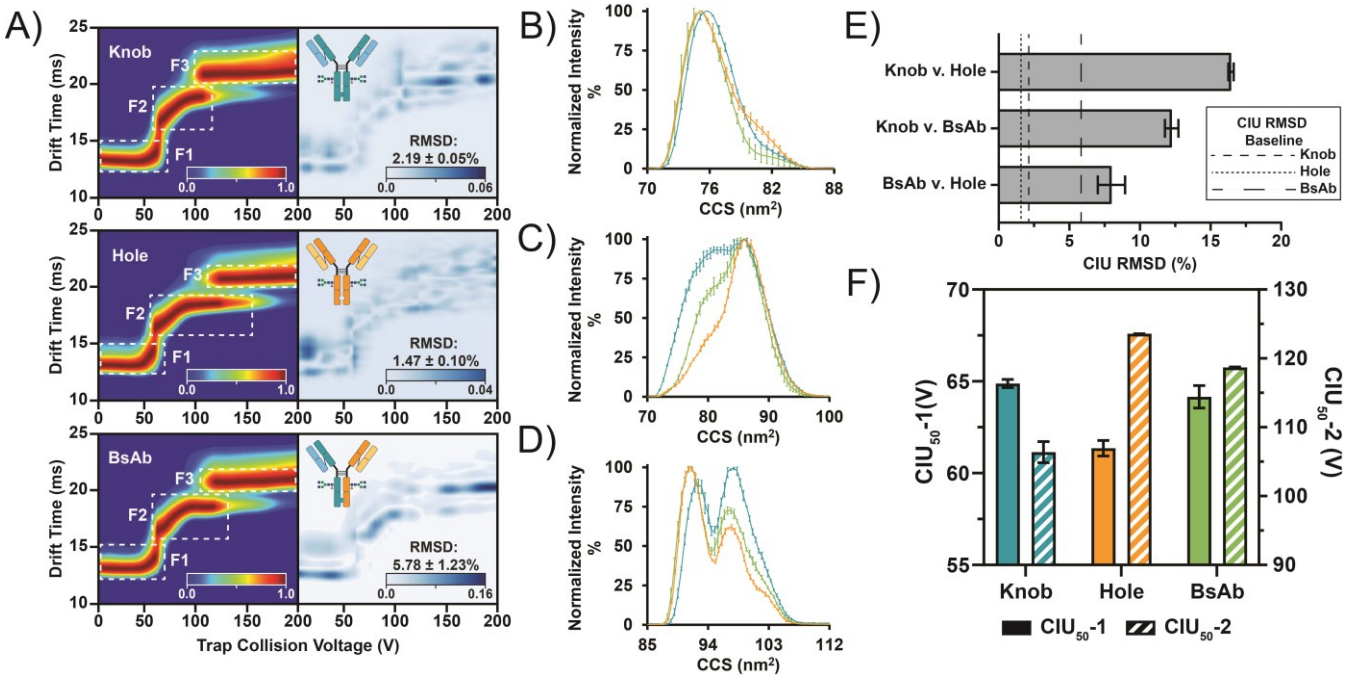

Figure 1. CIU experiments of native, unmodified knob (blue) and hole (orange) homodimers and KiH bsAb heterodimer (green). (A) Averaged CIU fingerprints (n = 3) for the 24^+ charge state (left) with corresponding replicate RMSD baselines (right). All fingerprints show three main features indicated by the dashed white boxes. Normalized $^{TW}CCS_{N2}$ distributions at (B) 5 V, (C) 65 V, (D) 110 V. At lower activation potentials, all antibodies adopt similar CCS distributions, which significantly diverge at higher acceleration potentials. (E) Pairwise RMSD analysis reveals global HOS differences among antibodies compared to replicate RMSD baselines (dashed lines). (F) CIU_{50} analysis illustrates how the model KiH bsAb adopts a stability between those of knob and hole homodimers.

Native MS Analysis. High resolution native MS experiments were performed on a standard commercial Q Exactive Orbitrap MS with Ultra High Mass Range (UHMR) platform (Thermo Scientific, San Jose, CA). Samples were further diluted to ~2 μM before analysis. Sample (~3 μL) was transferred to a gold-coated borosilicate capillary needle (prepared in house), and ions were generated via direct infusion using a commercial Thermo Fisher Nanospray Flex Ion Source (ES071) with a static nanospray ionization (NSI) probe operated in positive ion mode. Capillary voltages were held at 1.1 – 1.2 kV, and the inlet capillary was heated to 275°C. Nitrogen was used as the collision gas, and the trapping pressure was set to 3. Low *m/z* detector optimization and high *m/z* transfer optics were used to optimize the transmission of mAb homodimer and KiH bsAb heterodimer ions. In-source trapping was enabled with the desolvation voltage fixed at -50 V for improved ion transmission and efficient salt adduct removal. Transient times were set at 128 ms (resolution of 25,000 at *m/z* 400). Mass spectra were then processed and deconvoluted using UniDec software.[40]

Native IM-MS and CIU. IM-MS and CIU experiments were performed using a quadrupole-ion mobility-time-of-flight mass spectrometer (Q-IM-ToF-MS) instrument (Synapt G2 HDMS, Waters, Milford, MA). Sample (~3 μL) was transferred to a gold-coated borosilicate capillary needle, and ions were generated by direct infusion utilizing a nano-electrospray ionization (nESI) source set to the positive mode. The nESI capillary was operated at voltages of 1.1 – 1.5 kV. For intact and halfmer species, the sampling cone was operated at 40 V, while for Fab and Fc fragments, it was operated at 20 V to prevent in-source activation. The backing pressure was set to ~7.3 to 7.5 mbar. The helium cell flow rate was operated at 200 mL/min and pressurized to 1.4 x 10-3 mbar. The trap travelling wave ion guide was pressurized to 4.9 x 10-2 mbar of argon gas. The travelling-wave IM separator was operated at a pressure of ~3.4 mbar, and IM separation was achieved with a travelling wave height and velocity of 40 V and 600 m/s, respectively. The ToF-MS was operated over an m/z range of 1000 – 12,000 at a pressure of 2.3 x 10^{-6}. Ions were subjected to collisions in the travelling-wave ion trap prior to IM separation to perform CIU. For intact KiH bsAb, knob, and hole constructs, tandem-MS was utilized to select charge state 24^+. For ions corresponding to halfmer, charge state 16^+ was selected. The collisional voltages were then ramped from 5 V to 200V in 5 V intervals to construct each CIU fingerprint. For Fab and Fc fragment measurements, charge state 13^+ was selected, and collision voltages were ramped from 5 V to 140 V in 5 V increments since collisional activation above 140 V resulted in fragmentation. Polyalanine ions, bovine serum albumin, and glutamate dehydrogenase were used as CCS calibrants. All data collection was performed in triplicate.

IM and MS data were viewed using DriftScope and Masslynx V4.1 software, respectively (Waters, Milford, MA). Mass spectra were deconvoluted using UniDec software.[40] Drift times were extracted at each collision voltage using TWIMExtract (v1.5).[41] $^{TW}CCS_{N2}$ calculations were performed using IMSCal software.[42] Extracted drift time data were then analyzed using a home-built software package, CIUSuite 2 (v2.2).[43] CIU fingerprints were 2-D smoothed with a Savitzky-Golay function with a smoothing window of 5 and 2

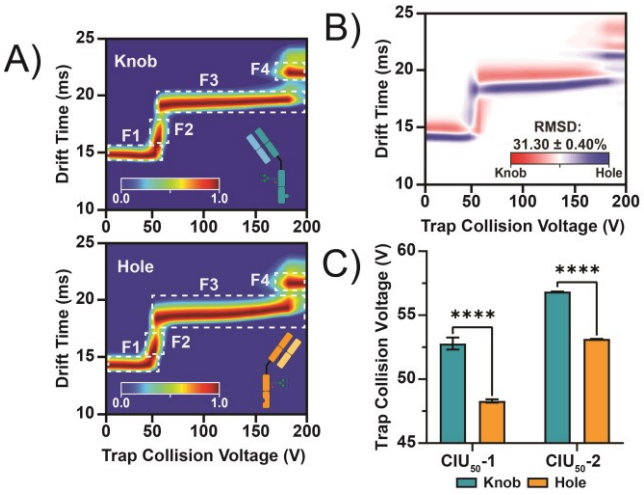

Figure 2. CIU data recorded for knob and hole halfmers. (A) Averaged CIU fingerprints (n = 3) for 16^+ charge states. (B) Pairwise RMSD analyses reveal significant differences between halfmer HOSs. (C) CIU_{50} analysis shows significant differences (**** $p < 0.0001$) in protein stabilities.

smoothing iterations. The collision voltage axis was interpolated with an axis scaling factor of 2 for intact constructs and 4 for halfmers and Fab and Fc fragments. Standard feature detection was performed using a minimum feature length of 3 steps, an allowed width of 0.75 drift time axis units, and a maximum CV gap length of 0. CIU_{50} values were then assigned using max centroiding mode with a transition region padding of 15 CV and a maximum CV gap length of 0. CIU_{50} represents the collision voltage at which 50% of a more compact state of the antibody transitions to a more unfolded state, and it defines the midpoint between adjacent features. Root-mean-square-deviation analysis (RMSD) analysis was performed using the compare function in CIUSuite 2. All CIU fingerprints shown are the average of three replicates.

Results and Discussion

Native IM-MS and CIU of knob and hole homodimers and KiH bsAb heterodimer. The native IM-MS spectra of knob, hole, and KiH bsAb samples reveal various ion populations corresponding to intact homodimer and heterodimer, as well as low and high molecular weight species (Figure S1A). Knob and hole spectra show high abundances of halfmers, highlighting that KiH mutations (knob: T366W, hole: T366S, L368A, Y407V) impede efficient halfmer dimerization into homodimer. Size-exclusion chromatography with multi-angle light scattering (SEC-MALS) data showed mass fractions of ~56% and ~43% for homodimers and halfmers, respectively (Figure S2). Differences in halfmer abundances in our native IM-MS data are likely the result of ionization efficiency differences between the two ion classes tracked in these experiments. IM-MS data for the KiH bsAb, on the other hand, shows very minimal halfmer populations, revealing the effective association of knob and hole halfmers into heterodimer. All intact antibodies present narrow charge state distributions (21^+ to 26^+), indicating the preservation of native-like structural information in the gas-phase compared to denatured species.[44–46] Moreover, all glycosylation sites are conserved for each antibody, and averaged deconvoluted masses include all glycoforms

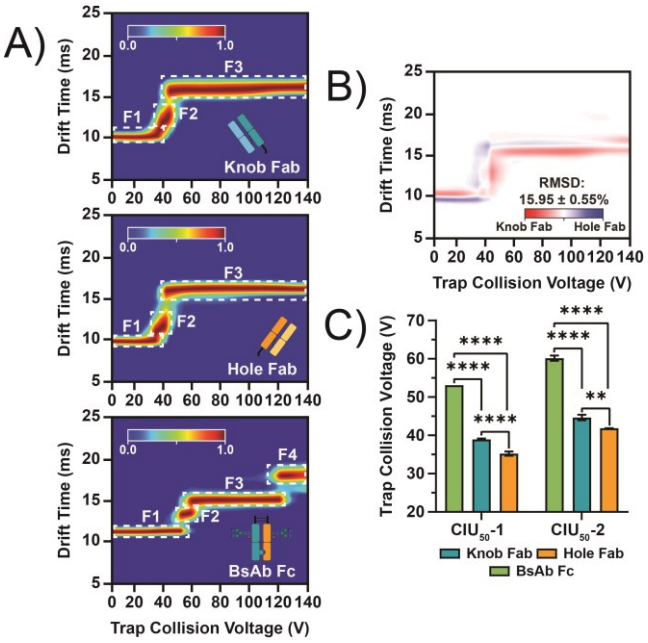

Figure 3. CIU data recorded for Fab and Fc fragments. (A) Averaged CIU fingerprints (n = 3) for 13^+ charge states. (B) Pairwise RMSD analysis reveals significant differences between knob and hole Fab fragments. (C) CIU_{50} analysis indicates significant differences (** $p < 0.01$, **** $p < 0.0001$) in fragment stabilities.

such as those commonly found in standard mAbs (Figure S1B).

To further probe the HOS of knob and hole homodimers and KiH bsAb heterodimer, we performed CIU on a range of charge states (22^+ to 24^+). Previous studies have indicated that ion charge state influences the number of transitions in its CIU fingerprint, where lower charge states produce CIU data that correlates with the number of protein domains[47,48] As expected, the lowest charge state, 22^+, requires higher acceleration voltages to unfold, giving rise to fewer CIU intermediates when compared to more highly-charged ions (Figure S3). We observe three main CIU features for 23^+ and 24^+ KiH bsAb ions, where the intensity of the most unfolded feature detected at higher collision voltages is most prominent in the latter charge state. For our analyses described below, we chose to focus on 24^+ ions due to their large relative intensities and more prominent third CIU features. Globally, our analysis reveals both similarities and differences across the parent homodimer mAbs and the KiH bsAb studied here (Figure 1). Notably, all antibodies undergo a similar number of CIU transitions. Technical replicates produce baseline RMSDs of < 6%, which indicate consistent, reproducible CIU data for all samples (Figure 1A). To better quantify differences among our intact constructs, we first utilized the classification workflow within CIUSuite 2 to select collision voltages that exhibit the greatest differences in arrival time distributions (ATDs) between CIU fingerprints.[43,49] Conversion of IM drift times to $^{TW}CCS_{N2}$ values reveal broad CCS ensembles that are essentially indistinguishable by IM-MS alone at 5 V (Figure 1B). However, CCS data captured at collision voltages of 65 V (Figure 1C) and 110 V (Figure 1D), reveal significantly different distributions of $^{TW}CCS_{N2}$. At these higher collision voltages, we observe that the KiH bsAb occupies an intermediate space of $^{TW}CCS_{N2}$

values between those of knob and hole homodimer mAbs, which agrees with previous CIU findings of a bsAb formed via FAE.[39] Interestingly, the $^{TW}CCS_{N2}$ distributions recorded for the KiH bsAb at 65 V are similar to those produced by knob homodimer CIU data. At 110 V, however, KiH bsAb CIU data switches to produce $^{TW}CCS_{N2}$ distributions like those of hole homodimer CIU data. These observations provide early evidence suggesting bsAb stability is discreetly connected to both parent homodimer mAbs for the KiH model studied here.

To build upon these observations, we performed pairwise RMSD analyses between CIU data recorded for all antibodies in order to probe global conformational differences (Figure 1E). A comparison of knob and hole homodimers yields an RMSD of 16.45 ± 0.19%, indicating significant differences in global homodimer mAb HOS. When CIU data collected for knob and hole homodimers are compared to KiH bsAb data, however, we observe decreased RMSD values. Specifically, a comparison between knob homodimer and the KiH bsAb CIU fingerprints produces an RMSD of 12.25 ± 0.48%, while a comparison between hole homodimer and the KiH bsAb produces an RMSD of 7.98 ± 0.96% (Figure S4). These comparisons reveal that the KiH bsAb CIU data, and by extension bsAb global stability, most closely resembles that of the hole homodimer for the model system studied here. Next, we shifted our focus to evaluating differences in CIU_{50} based stability values between knob, hole, and KiH bsAb. CIU_{50} analyses of knob, hole, and KiH bsAb constructs indicate that KiH bsAb stability can indeed be characterized as intermediate between its parent homodimers if initial protein unfolding is used as the primary method of evaluating protein stability. Specifically, CIU_{50}-1 values, which correspond to the first CIU transition recorded in our fingerprints, indicate that the hole homodimer (61.36 ± 0.42 V) is less stable than both the knob homodimer (64.88 ± 0.23 V) and the KiH bsAb (64.16 ± 0.62 V) (Figure 1F). Conversely, CIU_{50}-2 values, which are linked to the second, higher-energy CIU transition detected in our experiments, reveal that the knob homodimer (106.38 ± 1.52 V) unfolds at collision voltages lower than those of both the hole homodimer (123.57 ± 0.02 V) and the KiH bsAb (118.67 ± 0.07 V). Our data indicates that the KiH bsAb studied here exhibits CIU-based composite stabilities of 51.4% knob and 48.6% hole for CIU_{50}-1 and 46.3% knob and 53.7% hole for CIU_{50}-2. We quantified these stability contributions by summing each CIU_{50} value of knob and hole together for each transition then divided each measured CIU_{50} by this total. Taken together, these results suggest that the CIU_{50}-1 and CIU_{50}-2 values recorded in our fingerprints are likely reporting on the local stabilities of different domains within the KiH bsAb and mAb constructs studied here.

Middle-level CIU reveals knob and hole domain contributions to KiH bsAb HOS. To better assign regions of the KiH bsAb to specific CIU features, we performed CIU experiments targeting antibody fragment ions generated under native conditions. First, we recorded CIU data for 16^+ knob and hole halfmers (Figure 2) present in our homodimer mAb IM-MS spectra (Figure S1A). In these fingerprints, we observe four main CIU features across both constructs, but RMSD analysis reveals significant differences in their native-like structures (31.30 ± 0.40%) when compared to baseline RMSD values recorded for technical replicates (3.02 ± 0.54% and 1.48 ± 0.23% for knob and hole halfmers, respectively). CIU_{50} analysis further reveals that knob halfmer is significantly more stable than the hole halfmer across the two unfolding transitions observed (Figure 2C). These differences in stability correlate strongly with our prior measurements of intact hole and knob homodimer CIU_{50}-1 values. We note that knob and hole halfmers differ in experimental mass by ~2%. Previous studies have demonstrated that protein primary structure can influence CIU patterns.[47] Therefore, it is likely that the differences we observe in knob and hole halfmer stability are connected, in part, to the sequence differences associated with each halfmer. We hypothesize that the Fab regions, which contain hypervariable complementarity-determining regions (CDRs) that determine specific antigen binding, are the main contributors to the differences in CIU detected in our data.

To continue our efforts in assigning CIU features observed in the KiH bsAb to specific domains or regions within its structure, we performed CIU on the Fab and Fc fragments generated via papain digestion. Here, papain cleaves above the hinge region to produce a knob Fab, a hole Fab, and a chimeric Fc held together by hinge disulfides and non-covalent interactions (Figure S5). CIU fingerprints for Fab fragments reveal three CIU features for both knob and hole Fabs (Figure 3). The CIU fingerprint of the chimeric Fc domain, on the other hand, shows four CIU features. Although IM-MS and CIU of middle-level fragments of mAbs have been performed previously, most involved $F(ab')_2$ and non-covalent Fc produced via IdeS digestion.[34,36,50] Botzanowski and coworkers, in particular, described a compaction phase in non-covalent Fc CIU data at higher collision voltages.[50] Notably, we do not observe a compaction phase in our Fc CIU fingerprint, indicating that the fragments studied here are not directly comparable to those previously reported in the literature. As such, these CIU experiments provide new insights into individual Fab and Fc HOS and stability for KiH bsAbs. Technical replicates recorded for knob Fab, hole Fab, and chimeric Fc fragments yield RMSD baselines of 2.08 ± 0.28%, 1.41 ± 0.21%, and 4.85 ± 0.70%, respectively. Although knob and hole Fabs share qualitatively similar CIU fingerprints, difference analysis reveals an RMSD of 15.59 ± 0.55%, indicating that these fragments differ greatly in terms of their HOS. Like our halfmer data, we note that the Fabs studied here differ in mass by ~2%. Thus, the differences in HOS that we observe are most likely connected to the hypervariable regions of the CDRs of each Fab. Furthermore, a stability assessment of these fragments quantitatively shows that the knob Fab is significantly more stable than the Hole Fab across both CIU_{50}-1 and CIU_{50}-2 values recorded (Figure 3C). Interestingly, our data also indicate that the Fc domain is significantly more stable than both knob and hole Fab domains. This difference in stability is most likely related to the strong non-covalent interactions that exist between the C_H3 domains within each heavy chain, as well as the knob and hole mutations promoting heavy chain dimerization.[51–53]

Removal of *N*-glycans impact knob and hole homodimer and KiH bsAb heterodimer conformation and stability. Previous work has demonstrated that CIU is sensitive to different levels of mAb glycosylation, where the removal of sugars leads to the destabilization of mAb HOS.[33–35] Furthermore, the removal of glycans has been shown to decrease

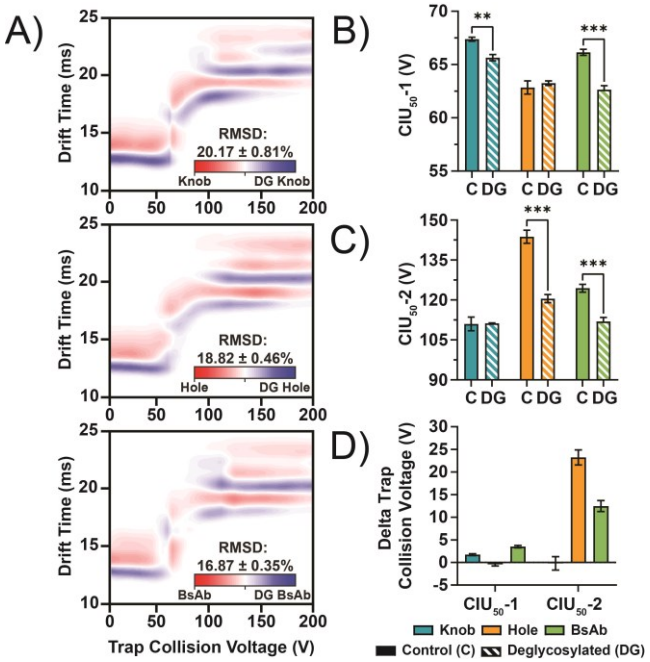

Figure 4. CIU of deglycosylated knob and hole homodimers and KiH bsAb heterodimer 24^+ ions (n = 3). (A) RMSD analysis comparing control and deglycosylated antibodies reveals significant differences in HOS. (B) CIU_{50}-1 and (C) CIU_{50}-2 analysis reveals significant destabilization of antibodies after deglycosylation (** p < 0.01, *** p < 0.001). (D) Plot of differences in CIU_{50} values between control and deglycosylated antibodies.

the thermal stability of C_H2 domains within the mAb Fc region.[54] Therefore, to better assign CIU transitions corresponding to the unfolding of the Fc domain of our model KiH bsAb, we removed *N*-linked glycans from the C_H2 domains of knob, hole, and KiH bsAb constructs and probed their resulting stabilities using CIU.

To better track the progress of our deglycosylation reactions, we performed high-resolution native orbitrap MS experiments to resolve individual homodimer mAb and KiH bsAb glycoforms both prior to and after the addition of PNGase F. Our results provide evidence for a wide range of glycoforms for knob, hole, and KiH bsAb constructs. Notably, the KiH bsAb exhibits high glycan heterogeneity, containing at least 12 different glycoforms (Figure S6). This observation is most likely attributed to the unique glycan populations present on each separate knob and hole heavy chain in the assembled KiH bsAb, further increasing its complexity. Specifically, we not only observe mass shifts of 162 Da, corresponding to a hexose, but also shifts of 291 Da, corresponding to either a *N*-acetyl neuraminic acid (Neu5Ac) or a sialic acid. In contrast, knob and hole homodimer glycoforms differ primarily by 162 Da, with the knob homodimer native MS containing a single 291 Da shift in the mAb glycoforms detected. Glycan removal results in average mass shifts of 4362.4 ± 336.8, 2121.8 ± 210.6, and 3854.7 ± 654.0 Da for knob, hole, and KiH bsAb constructs, respectively, all in line with expectations for PNGase F deglycosylation.[34] The variability observed in the homodimer mAb or KiH bsAb mass lost following PNGase F treatment is a reflection of the unique glycosylation patterns observed for each antibody studied here.

CIU experiments for both control and deglycosylated antibodies reveal the same number of features as those observed in our initial CIU data, alongside clear shifts in protein stability. RMSD analysis reveals significant differences between control and deglycosylated forms (~17 – 20%) compared to baseline RMSDs of < 4% (Figure 4A). Pre-CIU IM drift times for our deglycosylated homodimer mAbs and KiH bsAb are universally shorter than those produced by control (glycosylated) antibodies and thus produce CIU intermediates that are similarly shifted. Interestingly, an RMSD analysis comparing deglycosylated knob, hole, and KiH bsAb constructs reveals that the deglycosylated bsAb most closely resembles the deglycosylated hole homodimer (Figure S7), a result that agrees well with our initial CIU experiments on the glycosylated forms of these antibodies discussed above (Figure 1).

A quantitative analysis of CIU_{50} data reveals an asymmetric effect on protein stability upon the removal of glycans from each antibody (Figure 4 B,C). CIU_{50}-1 values point to a significant decrease in gas-phase stability for deglycosylated knob homodimer (65.65 ± 0.28 V) and KiH bsAb (62.65 ± 0.37 V) when compared to controls (73.35 ± 0.36 V and 66.15 ± 0.28 for knob homodimer and KiH bsAb, respectively). Deglycosylated hole homodimer, on the other hand, shows no detectable change in CIU_{50}-1. In comparison, our CIU_{50}-2 results point to a significant decrease in stability for deglycosylated hole homodimer (120.50 ± 1.53 V) and KiH bsAb (111.94 ± 1.46 V) compared to controls (143.73 ± 2.44 V and 124.41 ± 1.49 V for hole homodimer and KiH bsAb, respectively), with no change observed in knob CIU_{50}-2. By plotting the differences in CIU_{50} recorded between our control and deglycosylated antibodies, we can delineate which CIU transition is most affected by deglycosylation (Figure 4D). Overall, we observe greater differences in CIU_{50}-2 when compared to CIU_{50}-1, with the latter transition shifting < 5V (maximally ~6%) across all applicable constructs and the former generating shifts of 10 – 25 V (maximally ~17%). We note that the knob homodimer exhibits a destabilized CIU_{50}-2 when compared with both bsAb and hole constructs even before deglycoyslation as discussed above. Previously, the resolved structure of another model knob-knob Fc has shown that knob-knob Fc is destabilized due to a change in the relative orientation of C_H3 domains provoked by the knob point mutation.[55] Therefore, it is possible that the T366W mutation in the C_H3 domains of knob heavy chains is affecting the non-covalent interactions at the C_H3-C_H3 interface of the knob homodimer, permitting flexibility and leading to lower CIU_{50}-2 values.

Conclusions

Here, we demonstrate the capabilities of IM-MS in combination with CIU to establish HOS connections between a model KiH bsAb and its parent homodimer mAbs. We found CCS alone to be insufficient to resolve the subtle HOS differences between the antibodies studied here. In contrast, CIU fingerprints permitted us to resolve and differentiate each iso-cross-sectional antibody. Overall, our findings indicate that our model KiH bsAb adopts an intermediate cross-sectional and stability profile between those of its parent knob and hole homodimer mAbs, an observation driven by stability contributions of each parent halfmer to KiH bsAb stability.

Importantly, our analysis of a model KiH bsAb and its parent mAbs has enabled us to assign many details surrounding the CIU of a model KiH bsAb for the first time. By studying mAb and bsAb fragments, alongside deglycosylated constructs, our data strongly point to the first and second CIU transitions of the KiH bsAb and the parent mAbs in this work to be related to Fab and Fc domains unfolding, respectively. In particular, the CIU profiles recorded for Fab fragments in comparison to liberated chimeric Fc domains indicated lesser stabilities for the Fab domains in a manner that reflected their relative stabilities in larger constructs (*e.g.* halfmers and homodimers). The larger stability of the Fc, in combination with the larger influence of deglycosylation on CIU_{50}-2, supports the notion that higher-energy CIU transitions in the KiH bsAb are related to Fc CIU, while lower energy transitions are connected to Fab CIU. A greater degree of granularity can be assigned to KiH bsAb CIU than the generalities detailed above, which we argue are likely applicable to all mAb CIU collected for ions having sufficiently lower charge states. For this work's model KiH bsAb, our results indicate that the lower energy, Fab dominated, unfolding event is likely driven by the stability of the hole Fab domain, which all of our CIU data indicates is the least stable element of the KiH bsAb construct, and subsequent higher-energy CIU transitions are related to CH_2 and CH_3 domains within the knob-containing portion of the Fc. However, we acknowledge that these findings offer a simple explanation of the gas-phase unfolding mechanism of a model KiH bsAb. Future work will target the thorough evaluation of bsAb and mAb CIU pathways. Comparisons of KiH bsAbs constructed using different IgG subclasses, for instance, would provide further information regarding KiH bsAb stability.

Our ability to interpret the details of bsAb CIU, coupled with our enhanced understanding of the biophysical underpinnings of a model KiH bsAb's stability, has the potential to provide critical information in support of KiH bsAb discovery and development. Future work in our group aims to further develop IM-MS and CIU workflows to rapidly probe the suitability and HOS details of KiH bsAb construction. For example, we foresee combined native MS, IM-MS and CIU, available in a high-throughput mode, to reveal changes in KiH bsAb conformational dynamics and stability provoked changes in protein sequence, enabling us to relate HOS changes to overall KiH bsAb fitness for subsequent development efforts.

ASSOCIATED CONTENT

Supporting Information

The Supporting Information is available free of charge on the ACS Publications website.

IM-MS spectra and theoretical and experimental masses knob, hole, and KiH bsAb; CIU fingerprints for 22^+ - 24^+ ions of intact knob, hole, and KiH bsAb; RMSD plots of 24^+ ions; papain digestion cleavage site, papain digest IM-MS spectra, and theoretical and experimental masses of papain generated fragments; high-resolution spectra of knob, hole, and bsAb; CIU fingerprints and RMSD analysis of degylcosylated 24^+ ions.

AUTHOR INFORMATION

Corresponding Author

Brandon T. Ruotolo – *Department of Chemistry, University of Michigan, Ann Arbor, Michigan 48109, United States;* Phone: 1-734-6150198; Email: bruotolo@umich.edu; Fax: 1-734-615-3718

Authors

Rosendo C. Villafuerte-Vega – *Department of Chemistry, University of Michigan, Ann Arbor, Michigan 48109, United States*
Henry Li – *Department of Chemistry, University of Michigan, Ann Arbor, Michigan 48109, United States*
Thomas Slaney – *Biologics Department, Bristol Myers Squibb, New Brunswick, New Jersey 08903, United States*
Naresh Chennamsetty – *Biologics Department, Bristol Myers Squibb, New Brunswick, New Jersey 08903, United States*
Guodong Chen – *Biologics Department, Bristol Myers Squibb, New Brunswick, New Jersey 08903, United States*
Li Tao – *Biologics Department, Bristol Myers Squibb, New Brunswick, New Jersey 08903, United States*

Author Contributions

B.T. R., T.S., G. C., and L.T. designed and conceived of the experiments described. R.V.V. collected Synapt G2 and UHMR data and drafted the manuscript. B.T.R and R.V.V. analyzed all data. H.L. assisted in collecting and analyzing Synapt G2 data. T.S., N.C., G.G., and L.T. provided all antibodies used in this work. The manuscript was written through contributions of all authors. All authors have given approval to the final version of the manuscript.

Notes

The authors declare no competing financial interest.

ACKNOWLEDGMENT

This work is supported through funding provided by Bristol Myers Squibb, the UM Biosciences Initiative in support of the UM Biological Mass Spectrometry Facility, and the National Science Foundation (NSF, 1808541), supplied by the Chemical Measurement and Imaging Program in the Division of Chemistry, with partial co-funding from the Division of Molecular and Cellular Biosciences.

REFERENCES

(1) Segal, D. M.; Weiner, G. J.; Weiner, L. M. Bispecific Antibodies in Cancer Therapy. *Curr. Opin. Immunol.* **1999**, *11* (5), 558–562. https://doi.org/10.1016/S0952-7915(99)00015-1.

(2) Li, B.; Xu, L.; Pi, C.; Yin, Y.; Xie, K.; Tao, F.; Li, R.; Gu, H.; Fang, J. CD89-Mediated Recruitment of Macrophages via a Bispecific Antibody Enhances Anti-Tumor Efficacy. *Oncoimmunology* **2018**, *7* (1). https://doi.org/10.1080/2162402X.2017.1380142.

(3) Bacac, M.; Fauti, T.; Sam, J.; Colombetti, S.; Weinzierl, T.; Ouaret, D.; Bodmer, W.; Lehmann, S.; Hofer, T.; Hosse, R. J.; Moessner, E.; Ast, O.; Bruenker, P.; Grau-Richards, S.; Schaller, T.; Seidl, A.; Gerdes, C.; Perro, M.; Nicolini, V.; Steinhoff, N.; Dudal, S.; Neumann, S.; Von Hirschheydt, T.; Jaeger, C.; Saro, J.; Karanikas, V.; Klein, C.; Umaña, P. A Novel Carcinoembryonic Antigen T-Cell Bispecific Antibody (CEA TCB) for the Treatment of Solid Tumors. *Clin. Cancer Res.* **2016**, *22* (13), 3286–3297. https://doi.org/10.1158/1078-0432.CCR-15-1696.

(4) Atwal, J. K.; Chen, Y.; Chiu, C.; Mortensen, D. L.; Meilandt, W. J.; Liu, Y.; Heise, C. E.; Hoyte, K.; Luk, W.; Lu, Y.; Peng, K.; Wu, P.; Rouge, L.; Zhang, Y.; Lazarus, R. A.; Scearce-Levie, K.; Wang, W.; Wu, Y.; Tessier-Lavigne, M.; Watts, R. J. A Therapeutic Antibody Targeting BACE1 Inhibits Amyloid-β Production in Vivo. *Sci. Transl. Med.* **2011**, *3* (84), 84ra43. https://doi.org/10.1126/scitranslmed.3002254.

(5) Yu, Y. J.; Atwal, J. K.; Zhang, Y.; Tong, R. K.; Wildsmith, K. R.; Tan, C.; Bien-Ly, N.; Hersom, M.; Maloney, J. A.; Meilandt, W. J.; Bumbaca, D.; Gadkar, K.; Hoyte, K.; Luk, W.; Lu, Y.; Ernst, J. A.; Scearce-Levie, K.;

Couch, J. A.; Dennis, M. S.; Watts, R. J. Therapeutic Bispecific Antibodies Cross the Blood-Brain Barrier in Nonhuman Primates. *Sci. Transl. Med.* **2014**, *6* (261), 61ra154. https://doi.org/10.1126/scitranslmed.3009835.

(6) Chakravarthy, U.; Bailey, C.; Brown, D.; Campochiaro, P.; Chittum, M.; Csaky, K.; Tufail, A.; Yates, P.; Cech, P.; Giraudon, M.; Delmar, P.; Szczesny, P.; Sahni, J.; Boulay, A.; Nagel, S.; Fürst-Recktenwald, S.; Schwab, D. Phase I Trial of Anti–Vascular Endothelial Growth Factor/Anti-Angiopoietin 2 Bispecific Antibody RG7716 for Neovascular Age-Related Macular Degeneration. *Ophthalmol. Retin.* **2017**, *1* (6), 474–485. https://doi.org/10.1016/j.oret.2017.03.003.

(7) Regula, J. T.; Lundh von Leithner, P.; Foxton, R.; Barathi, V. A.; Chui Ming, G. C.; Tun, S. B. B.; Wey, Y. S.; Iwata, D.; Dostalek, M.; Moelleken, J.; Stubenrauch, K. G.; Nogoceke, E.; Widmer, G.; Strassburger, P.; Koss, M. J.; Klein, C.; Shima, D. T.; Hartmann, G. Targeting Key Angiogenic Pathways with a Bispecific Cross MA b Optimized for Neovascular Eye Diseases. *EMBO Mol. Med.* **2016**, *11* (8), 1265–1288. https://doi.org/10.15252/emmm.201505889.

(8) Ma, J.; Mo, Y.; Tang, M.; Shen, J.; Qi, Y.; Zhao, W.; Huang, Y.; Xu, Y.; Qian, C. Bispecific Antibodies: From Research to Clinical Application. *Front. Immunol.* **2021**, *12*. https://doi.org/10.3389/fimmu.2021.626616.

(9) Labrijn, A. F.; Janmaat, M. L.; Reichert, J. M.; Parren, P. W. H. I. Bispecific Antibodies: A Mechanistic Review of the Pipeline. *Nat. Rev. Drug Discov.* **2019**, *18*, 585–608. https://doi.org/10.1038/s41573-019-0028-1.

(10) Kontermann, R. E.; Brinkmann, U. Bispecific Antibodies. *Drug Discov. Today* **2015**, *20* (7), 838–847. https://doi.org/10.1016/j.drudis.2015.02.008.

(11) Klein, C.; Sustmann, C.; Thomas, M.; Stubenrauch, K.; Croasdale, R.; Schanzer, J.; Brinkmann, U.; Kettenberger, H.; Regula, J. T.; Schaefer, W. Progress in Overcoming the Chain Association Issue in Bispecific Heterodimeric IgG Antibodies. *mAbs*. 2012, pp 653–663. https://doi.org/10.4161/mabs.21379.

(12) Ridgway, J. B. B.; Presta, L. G.; Carter, P. "Knobs-into-Holes" Engineering of Antibody C(H)3 Domains for Heavy Chain Heterodimerization. *Protein Eng.* **1996**, *9* (7), 617–621. https://doi.org/10.1093/protein/9.7.617.

(13) Zhou, Q.; Qiu, H. The Mechanistic Impact of N-Glycosylation on Stability, Pharmacokinetics, and Immunogenicity of Therapeutic Proteins. *J. Pharm. Sci.* **2019**, *108* (4), 1366–1377. https://doi.org/10.1016/j.xphs.2018.11.029.

(14) Dingman, R.; Balu-Iyer, S. V. Immunogenicity of Protein Pharmaceuticals. *J. Pharm. Sci.* **2019**, *108* (5), 1637–1654. https://doi.org/10.1016/j.xphs.2018.12.014.

(15) Hermeling, S.; Crommelin, D. J. A.; Schellekens, H.; Jiskoot, W. Structure-Immunogenicity Relationships of Therapeutic Proteins. *Pharm. Res.* **2004**, *21* (6), 897–903. https://doi.org/10.1023/B:PHAM.0000029275.41323.a6.

(16) Roberts, C. J. Therapeutic Protein Aggregation: Mechanisms, Design, and Control. *Trends Biotechnol.* **2014**, *32* (7), 372–380. https://doi.org/10.1016/j.tibtech.2014.05.005.

(17) Gabrielson, J. P.; Weiss, W. F. Technical Decision-Making with Higher Order Structure Data: Starting a New Dialogue. *J. Pharm. Sci.* **2015**, *104* (4), 1240–1245. https://doi.org/10.1002/jps.24393.

(18) Berkowitz, S. A.; Engen, J. R.; Mazzeo, J. R.; Jones, G. B. Analytical Tools for Characterizing Biopharmaceuticals and the Implications for Biosimilars. *Nat. Rev. Drug Discov.* **2012**, *11*, 527–540. https://doi.org/10.1038/nrd3746.

(19) Joshi, V.; Shivach, T.; Yadav, N.; Rathore, A. S. Circular Dichroism Spectroscopy as a Tool for Monitoring Aggregation in Monoclonal Antibody Therapeutics. *Anal. Chem.* **2014**, *86* (23), 11606–11613. https://doi.org/10.1021/ac503140j.

(20) Moreno, M. R.; Tabitha, T. S.; Nirmal, J.; Radhakrishnan, K.; Yee, C. H.; Lim, S.; Venkatraman, S.; Agrawal, R. Study of Stability and Biophysical Characterization of Ranibizumab and Aflibercept. *Eur. J. Pharm. Biopharm.* **2016**, *108*, 156–167. https://doi.org/10.1016/j.ejpb.2016.09.003.

(21) Goyon, A.; D'Atri, V.; Colas, O.; Fekete, S.; Beck, A.; Guillarme, D. Characterization of 30 Therapeutic Antibodies and Related Products by Size Exclusion Chromatography: Feasibility Assessment for Future Mass Spectrometry Hyphenation. *J. Chromatogr. B* **2017**, *1065–1066* (August), 35–43. https://doi.org/10.1016/j.jchromb.2017.09.027.

(22) Brinson, R. G.; Marino, J. P.; Delaglio, F.; Arbogast, L. W.; Evans, R. M.; Kearsley, A.; Gingras, G.; Ghasriani, H.; Aubin, Y.; Pierens, G. K.; Jia, X.; Mobli, M.; Grant, H. G.; Keizer, D. W.; Schweimer, K.; Ståhle, J.; Widmalm, G.; Zartler, E. R.; Lawrence, C. W.; Reardon, P. N.; Cort, J. R.; Xu, P.; Ni, F.; Yanaka, S.; Kato, K.; Parnham, S. R.; Tsao, D.; Blomgren, A.; Rundlöf, T.; Trieloff, N.; Schmieder, P.; Ross, A.; Skidmore, K.; Chen, K.; Keire, D.; Freedberg, D. I.; Suter-Stahel, T.; Wider, G.; llc, G.; Plavec, J.; Bradley, S. A.; Baldisseri, D. M.; Sforça, M. L.; Zeri, A. C. de M.; Wei, J. Y.; Szabo, C. M.; Amezcua, C. A.; Jordan, J. B.; Wikström, M. Enabling Adoption of 2D-NMR for the Higher Order Structure Assessment of Monoclonal Antibody Therapeutics. *MAbs* **2019**, *11* (1), 94–105. https://doi.org/10.1080/19420862.2018.1544454.

(23) Zheng, H.; Hou, J.; Zimmerman, M. D.; Wlodawer, A.; Minor, W. The Future of Crystallography in Drug Discovery. *Expert Opin. Drug Discov.* **2014**, *9* (2), 125–137. https://doi.org/10.1517/17460441.2014.872623.

(24) Hao, Y.; Yu, X.; Bai, Y.; Mcbride, H. J.; Huang, X. Cryo-EM Structure of HER2-Trastuzumab-Pertuzumab Complex. *PLoS One* **2019**, *14* (5), e0216095. https://doi.org/10.1371/journal.pone.0216095.

(25) Chen, G.; Tao, L.; Li, Z. Recent Advancements in Mass Spectrometry for Higher Order Structure Characterization of Protein Therapeutics. *Drug Discov. Today* **2022**, *27* (1), 196–206. https://doi.org/10.1016/j.drudis.2021.09.010.

(26) Strop, P.; Ho, W. H.; Boustany, L. M.; Abdiche, Y. N.; Lindquist, K. C.; Farias, S. E.; Rickert, M.; Appah, C. T.; Pascua, E.; Radcliffe, T.; Sutton, J.; Chaparro-Riggers, J.; Chen, W.; Casas, M. G.; Chin, S. M.; Wong, O. K.; Liu, S. H.; Vergara, G.; Shelton, D.; Rajpal, A.; Pons, J. Generating Bispecific Human IgG1 and IgG2 Antibodies from Any Antibody Pair. *J. Mol. Biol.* **2012**, *420* (3), 204–219. https://doi.org/10.1016/j.jmb.2012.04.020.

(27) Lewis, S. M.; Wu, X.; Pustilnik, A.; Sereno, A.; Huang, F.; Rick, H. L.; Guntas, G.; Leaver-Fay, A.; Smith, E. M.; Ho, C.; Hansen-Estruch, C.; Chamberlain, A. K.; Truhlar, S. M.; Conner, E. M.; Atwell, S.; Kuhlman, B.; Demarest, S. J. Generation of Bispecific IgG Antibodies by Structure-Based Design of an Orthogonal Fab Interface. *Nat. Biotechnol.* **2014**, *32* (2), 191–198. https://doi.org/10.1038/nbt.2797.

(28) Ruotolo, B. T.; Benesch, J. L. P.; Sandercock, A. M.; Hyung, S. J.; Robinson, C. V. Ion Mobility-Mass Spectrometry Analysis of Large Protein Complexes. *Nat. Protoc.* **2008**, *3* (7), 1139–1152. https://doi.org/10.1038/nprot.2008.78.

(29) Debaene, F.; Wagner-Rousset, E.; Colas, O.; Ayoub, D.; Corvaïa, N.; Van Dorsselaer, A.; Beck, A.; Cianférani, S. Time Resolved Native Ion-Mobility Mass Spectrometry to Monitor Dynamics of Igg4 Fab Arm Exchange and "Bispecific" Monoclonal Antibody Formation. *Anal. Chem.* **2013**, *85* (20), 9785–9792. https://doi.org/10.1021/ac402237v.

(30) Bagal, D.; Valliere-Douglass, J. F.; Balland, A.; Schnier, P. D. Resolving Disulfide Structural Isoforms of IgG2 Monoclonal Antibodies by Ion Mobility Mass Spectrometry. *Anal. Chem.* **2010**, *82* (16), 6751–6755. https://doi.org/10.1021/ac1013139.

(31) Debaene, F.; Bœuf, A.; Wagner-Rousset, E.; Colas, O.; Ayoub, D.; Corvaïa, N.; Van Dorsselaer, A.; Beck, A.; Cianférani, S. Innovative Native MS Methodologies for Antibody Drug Conjugate Characterization: High Resolution Native MS and IM-MS for Average DAR and DAR Distribution Assessment. *Anal. Chem.* **2014**, *86* (21), 10674–10683. https://doi.org/10.1021/ac502593n.

(32) Dixit, S. M.; Polasky, D. A.; Ruotolo, B. T. Collision Induced Unfolding of Isolated Proteins in the Gas Phase: Past, Present, and Future. *Curr. Opin. Chem. Biol.* **2018**, *42*, 93–100. https://doi.org/10.1016/j.cbpa.2017.11.010.

(33) Tian, Y.; Han, L.; Buckner, A. C.; Ruotolo, B. T. Collision Induced Unfolding of Intact Antibodies: Rapid Characterization of Disulfide Bonding Patterns, Glycosylation, and Structures. *Anal. Chem.* **2015**, *87* (22), 11509–11515. https://doi.org/10.1021/acs.analchem.5b03291.

(34) Tian, Y.; Ruotolo, B. T. Collision Induced Unfolding Detects Subtle Differences in Intact Antibody Glycoforms and Associated Fragments. *Int. J. Mass Spectrom.* **2018**, *425*, 1–9. https://doi.org/10.1016/j.ijms.2017.12.005.

(35) Upton, R.; Migas, L. G.; Pacholarz, K. J.; Beniston, R. G.; Estdale, S.; Firth, D.; Barran, P. E. Hybrid Mass Spectrometry Methods Reveal Lot-to-Lot Differences and Delineate the Effects of Glycosylation on the Tertiary Structure of Herceptin®. *Chem. Sci.* **2019**, *10* (9), 2811–2820. https://doi.org/10.1039/c8sc05029e.

(36) Watanabe, Y.; Vasiljevic, S.; Allen, J. D.; Seabright, G. E.; Duyvesteyn, H. M. E.; Doores, K. J.; Crispin, M.; Struwe, W. B. Signature of Antibody Domain Exchange by Native Mass Spectrometry and Collision-Induced Unfolding. *Anal. Chem.* **2018**, *90* (12), 7325–7331. https://doi.org/10.1021/acs.analchem.8b00573.

(37) Deslignière, E.; Ehkirch, A.; Duivelshof, B. L.; Toftevall, H.; Sjögren, J.; Guillarme, D.; D'atri, V.; Beck, A.; Hernandez-Alba, O.; Cianférani, S. State-of-the-Art Native Mass Spectrometry and Ion Mobility Methods to Monitor Homogeneous Site-Specific Antibody-Drug Conjugates Synthesis. *Pharmaceuticals* **2021**, *14* (6), 1–13. https://doi.org/10.3390/ph14060498.

(38) Tian, Y.; Lippens, J. L.; Netirojjanakul, C.; Campuzano, I. D. G.; Ruotolo, B. T. Quantitative Collision-Induced Unfolding Differentiates Model Antibody–Drug Conjugates. *Protein Sci.* **2019**, *28* (3), 598–608. https://doi.org/10.1002/pro.3560.

(39) Hernandez-Alba, O.; Wagner-Rousset, E.; Beck, A.; Cianférani, S. Native Mass Spectrometry, Ion Mobility, and Collision-Induced Unfolding for Conformational Characterization of IgG4 Monoclonal Antibodies. *Anal. Chem.* **2018**, *90* (15), 8865–8872. https://doi.org/10.1021/acs.analchem.8b00912.

(40) Marty, M. T.; Baldwin, A. J.; Marklund, E. G.; Hochberg, G. K. A.; Benesch, J. L. P.; Robinson, C. V. Bayesian Deconvolution of Mass and Ion Mobility Spectra: From Binary Interactions to Polydisperse Ensembles. *Anal. Chem.* **2015**, *87* (8), 4370–4376.

https://doi.org/10.1021/acs.analchem.5b00140.
(41) Haynes, S. E.; Polasky, D. A.; Dixit, S. M.; Majmudar, J. D.; Neeson, K.; Ruotolo, B. T.; Martin, B. R. Variable-Velocity Traveling-Wave Ion Mobility Separation Enhancing Peak Capacity for Data-Independent Acquisition Proteomics. *Anal. Chem.* **2017**, *89* (11), 5669–5672. https://doi.org/10.1021/acs.analchem.7b00112.
(42) Richardson, K.; Langridge, D.; Dixit, S. M.; Ruotolo, B. T. An Improved Calibration Approach for Traveling Wave Ion Mobility Spectrometry: Robust, High-Precision Collision Cross Sections. *Anal. Chem.* **2021**, *93* (7), 3542–3550. https://doi.org/10.1021/acs.analchem.0c04948.
(43) Polasky, D. A.; Dixit, S. M.; Fantin, S. M.; Ruotolo, B. T. CIUSuite 2: Next-Generation Software for the Analysis of Gas-Phase Protein Unfolding Data. *Anal. Chem.* **2019**, *91* (4), 3147–3155. https://doi.org/10.1021/acs.analchem.8b05762.
(44) Kafader, J. O.; Melani, R. D.; Schachner, L. F.; Ives, A. N.; Patrie, S. M.; Kelleher, N. L.; Compton, P. D. Native vs Denatured: An in Depth Investigation of Charge State and Isotope Distributions. *J. Am. Soc. Mass Spectrom.* **2020**, *31* (3), 574–581. https://doi.org/10.1021/jasms.9b00040.
(45) Chowdhury, S. K.; Katta, V.; Chait, B. T. Probing Conformational Changes in Proteins by Mass Spectrometry. *J. Am. Chem. Soc.* **1990**, *112* (24), 9012–9013. https://doi.org/10.1021/ja00180a074.
(46) Campuzano, I. D. G.; Robinson, J. H.; Hui, J. O.; Shi, S. D. H.; Netirojjanakul, C.; Nshanian, M.; Egea, P. F.; Lippens, J. L.; Bagal, D.; Loo, J. A.; Bern, M. Native and Denaturing Ms Protein Deconvolution for Biopharma: Monoclonal Antibodies and Antibody-Drug Conjugates to Polydisperse Membrane Proteins and Beyond. *Anal. Chem.* **2019**, *91* (15), 9472–9480. https://doi.org/10.1021/acs.analchem.9b00062.
(47) Eschweiler, J. D.; Martini, R. M.; Ruotolo, B. T. Chemical Probes and Engineered Constructs Reveal a Detailed Unfolding Mechanism for a Solvent-Free Multidomain Protein. *J. Am. Chem. Soc.* **2017**, *139* (1), 534–540. https://doi.org/10.1021/jacs.6b11678.
(48) Zhong, Y.; Han, L.; Ruotolo, B. T. Collisional and Coulombic Unfolding of Gas-Phase Proteins: High Correlation to Their Domain Structures in Solution. *Angew. Chem. Int. Ed.* **2014**, *53*, 9209–9212. https://doi.org/10.1002/anie.201403784.
(49) Polasky, D. A.; Dixit, S. M.; Vallejo, D. D.; Kulju, K. D.; Ruotolo, B. T. An Algorithm for Building Multi-State Classifiers Based on Collision-Induced Unfolding Data. *Anal. Chem.* **2019**, *91* (16), 10407–10412. https://doi.org/10.1021/acs.analchem.9b02650.
(50) Botzanowski, T.; Hernandez-Alba, O.; Malissard, M.; Wagner-Rousset, E.; Desligniére, E.; Colas, O.; Haeuw, J. F.; Beck, A.; Cianférani, S. Middle Level IM-MS and CIU Experiments for Improved Therapeutic Immunoglobulin Subclass Fingerprinting. *Anal. Chem.* **2020**, *92* (13), 8827–8835. https://doi.org/10.1021/acs.analchem.0c00293.
(51) Wozniak-Knopp, G.; Stadlmann, J.; Rüker, F. Stabilisation of the FC Fragment of Human IgG1 by Engineered Intradomain Disulfide Bonds. *PLoS One* **2012**, *7* (1), 1–11. https://doi.org/10.1371/journal.pone.0030083.
(52) Huber, R.; Deisenhofer, J.; Colman, P. M.; Matsushima, M.; Palm, W. Crystallographic Structure Studies of an IgG Molecule and an Fc Fragment. *Nature* **1976**, *264*, 415–420. https://doi.org/10.1038/264415a0.
(53) Zhang, H. M.; Li, C.; Lei, M.; Lundin, V.; Lee, H. Y.; Ninonuevo, M.; Lin, K.; Han, G.; Sandoval, W.; Lei, D.; Ren, G.; Zhang, J.; Liu, H. Structural and Functional Characterization of a Hole-Hole Homodimer Variant in a "Knob-Into-Hole" Bispecific Antibody. *Anal. Chem.* **2017**, *89* (24), 13494–13501. https://doi.org/10.1021/acs.analchem.7b03830.
(54) Zheng, K.; Bantog, C.; Bayer, R. The Impact of Glycosylation on Monoclonal Antibody Conformation and Stability. *MAbs* **2011**, *3* (6). https://doi.org/10.4161/mabs.3.6.17922.
(55) Kuglstatter, A.; Stihle, M.; Neumann, C.; Müller, C.; Schaefer, W.; Klein, C.; Benz, J. Structural Differences between Glycosylated, Disulfide-Linked Heterodimeric Knob-into-Hole Fc Fragment and Its Homodimeric Knob-Knob and Hole-Hole Side Products. *Protein Eng. Des. Sel.* **2017**, *30* (9), 649–656. https://doi.org/10.1093/protein/gzx041.

Insert Table of Contents artwork here

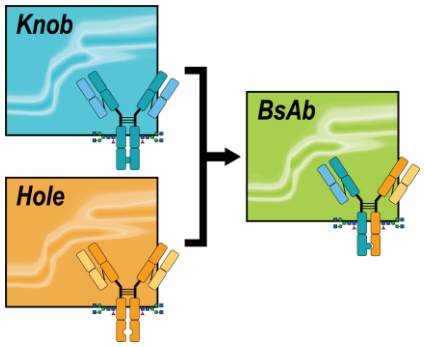

For Table of Contents Only